Laboratory generation of multiple periodic arrays of Alfvénic vortices

Cite as: Phys. Plasmas 32, 122109 (2025); doi: 10.1063/5.0298998
Submitted: 25 August 2025 · Accepted: 13 November 2025 ·
Published Online: 12 December 2025

W. Gekelman,[a] S. Vincena, and P. Pribyl

AFFILIATIONS

Department of Physics and Astronomy, University of California, Los Angeles, 475 Portola Plaza, Los Angeles, California 90095, USA

[a]Author to whom correspondence should be addressed: gekelman@physics.ucla.edu

ABSTRACT

A novel antenna has been constructed to generate shear Alfvén waves with large $k_\perp$ such that $k_\perp \simeq 1 - 6.5\,\mathrm{cm}^{-1}$. The antennas comprise multiple current loops, aligned with their normals transverse to the background magnetic field. Each loop is a generator of Alfvén cones. The observed spatial pattern is the interference of thousands of these cones. This is completely a linear effect; in the low-power regime of this experiment, the waves do not modify the plasma density or temperature. The cones overlap and the electric and magnetic fields associated with them can lead to stochastic motion of electrons and ions passing through them. This type of antenna can serve as a platform for the generation of magnetic Alfvénic turbulence. In this work, we present measurements in three dimensions of the wave magnetic fields and currents for several antennas and a pair of antennas. Close to the antennas, the wave number spectra match what is expected from the geometry of the antenna. In the region where the waves collide, additional modes are observed. At large wave amplitudes and large $k_\perp$, the ions can $\vec{E} \times \vec{B}$ drift from an "O" to an "X" point in the wave pattern and thereafter undergo stochastic motion.

I. INTRODUCTION

Large amplitude shear Alfvén waves have been the focus of experimental and theoretical research for decades. They are thought to play a large role in coronal heating,[1,2] and the solar wind.[3] The antennas developed for the present experiment can serve as a platform for the generation of magnetic Alfvénic turbulence, which is relevant, for example, to solar wind studies[4–6] and auroral physics.[7–9] Shear waves with magnetic field amplitudes of $\frac{\delta B}{B} \approx 0.1\%$–$0.2\%$ are the subject of many studies in the large plasma device[10] (LAPD) at the University of California, Los Angeles. The waves generate fast electrons which, in turn, increase the electron temperature.[11–13] Local temperature hot spots cause density depletions,[14] which may be wrongly attributed to the effects of the ponderomotive force. Electrons subject to Alfvénic turbulence can be heated by Landau damping.[15] There are many theoretical studies on the effects of the ponderomotive force of these waves.[16–22] Currently, there is no clear evidence of the effects of the ponderomotive force of shear Alfvén waves in the lab.

Fast electrons produced by large amplitude shear waves have been studied theoretically[23] and observed in the laboratory.[24] In the Earth's ionosphere, they are associated with the production of the aurora. Counter-streaming, large-amplitude Alfvén waves are thought to lead to Alfvén cascades in which a large number of daughter waves obeying a power spectrum are produced.[25–27]

When currents of the order of the electron skin depth oscillate so that $f_{osc} < f_{ci}$ Alfvén waves cones are generated.[28] This has been experimentally observed in both the kinetic regimes[29] ($V_A < v_{the}$) and inertial regimes[30] ($V_A > v_{the}$). Here v_{the} is the electron thermal velocity. The cones play an important role in the ionospheric Alfvén resonator[31,32] where cross field density gradients are present and solitary Alfvén waves are related to the cones. Alfvén cones may be related to solitary waves observed by spacecraft.[33,34]

To study chaotic motion of ions, or electrons, at first blush one might assume large ponderomotive fields or a cascade into turbulence is a requirement. This study involves the interference of a great number of Alfvén waves to generate interference patterns that contain a variety of perpendicular wave numbers and magnetic structures which resemble vorticies. The experiment is in the linear regime. Even so, the magnetic structure produced by the waves can, under the right conditions, lead to chaotic motion of ions. The antennas described here are agents of chaos.

A set of novel antennas was used to launch shear Alfvén waves with large perpendicular wave numbers (k_x, k_y) in a plane transverse to the background magnetic field ($\mathbf{B} = B_{0z}\hat{z}$). Alfvén waves with large perpendicular wave numbers can develop large parallel electric fields [Eq. (8)]. These, in turn, can drive current and scatter particles. Alfvén waves are expected to become nonlinear when the field fluctuations

$\frac{\delta B_\perp}{B_{0z}} \approx \frac{\lambda_\perp}{\tau V_A}$ where V_A is the Alfvén wave velocity, τ is the wave period, and B_{0z} the background magnetic field strength. To create waves in this regime, a specialized antenna "Alfvén tennis racket" was constructed and its performance will be discussed. The antenna has successfully generated two dimensional Alfvén vortices in planes transverse to B_0 with $k_\perp = 0.63\,\mathrm{cm}^{-1}$. Two types of secondary antenna were constructed to launch waves with different values of $k_\perp$. When both antennas are used simultaneously, they produce counter-propagating waves in the volume between them. The amplitude of the wave fields reported herein is well below the nonlinear threshold.

II. DESCRIPTION OF THE ANTENNAS

Two types of antenna were used. The first, labeled Antenna 1, is described as a "fork" and consisted of four vertical ceramic shafts (parallel to $\hat{\mathbf{y}}$) 22 cm long and 2.54 cm apart. This is similar to one that has been previously described.[35] Each strut was wound on a 6.4 mm diameter ceramic rod and had 240 turns of 1.3 mm diameter enameled copper magnet wire.[10] The assembly was covered with heat resistant epoxy. The background magnetic field of the LAPD is in the $\hat{\mathbf{z}}$ direction. Several "waffle" or "tennis racket" antennas labeled Antennas 2 and 3 were constructed to produce small perpendicular wavelengths in both transverse directions. Figure 1 shows an example of the construction of such a tennis racket with seven horizontal and vertical struts. The antennas that were actually used had an even number of struts—e.g., six or eight—because the odd number of windings produced a field that was dominated by an $n = 0$ mode. The rectangles formed by the intersections (one of which is outlined in blue in Fig. 1) had 48 turns (two layers of 24 turns) on each leg of the square and 288 turns on every horizontal and vertical leg. The figure shows gaps with coplanar vertical and horizontal legs. In practice, each leg was wound continuously on the ceramic with no gaps, with the horizontal and vertical legs stacked so that they were offset in the $\hat{\mathbf{z}}$ direction by the diameter of the ceramic (1 cm). The strut-to-strut phasing was determined by external connections. Two other antennas were constructed, one with six pairs of legs 5.4 cm apart (Antenna 3) and the second with seven pairs of legs (we only energized six pairs) 4 cm apart (Antenna 2). The antennas and vacuum wave numbers and wavelengths determined by the strut spacing are summarized in Table I.

Alfvén waves were produced with antennas A1 and A2, which were 195 cm apart. The magnetic field data were acquired on five planes transverse to the background magnetic field ($B_{0z} = 400$ G). An illustration of the placement of the two antennas in the LAPD is shown in Fig. 2.

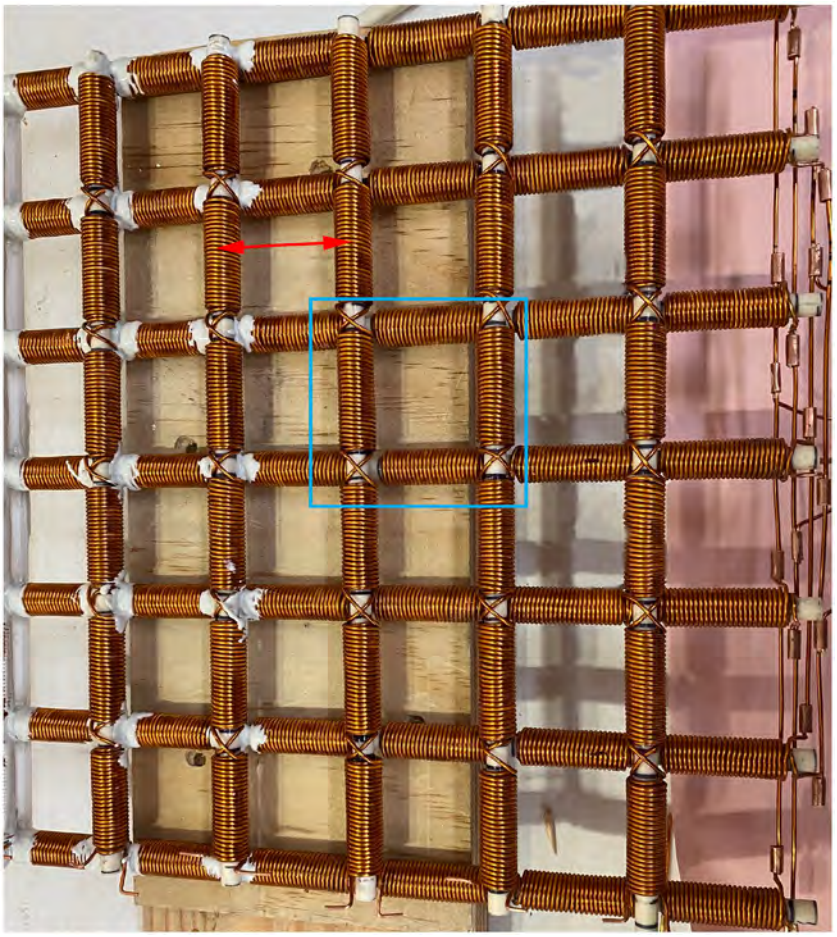

FIG. 1. Photograph of the first Alfvén tennis racket antenna before it was coated with epoxy. Phasing of the struts was controlled externally so that alternate ones were 180 degrees out of phase. The blue box illustrates one rectangular element of the antenna. The center to center distance between the struts was 4 cm. Antennas used in the experiment all had an even number of struts.

TABLE I. Vacuum wave numbers associated with the three antennas.

Antenna	k_x (cm^{-1})	k_y (cm^{-1})	λ_x (cm)	λ_y (cm)
A1 4 strap	2.47	0.29	2.54	22
A2 7 × 7	0.79	0.79	8.0	8.0
A3 6 × 6	1.2	1.2	5.4	5.4

The experiments were performed in the Large Plasma Device (LAPD) at UCLA.[1] The plasma column is 18 m long and 50 cm in diameter, and Helium plasma with density 5×10^{12} cm^{-3} $< n_e < 2 \times 10^{13}$ cm^{-3} was used. Helium neutrals were injected using two piezoelectric valves between the anode and the cathode. The gas puff and discharge length was 20 ms. The discharge was initiated with a custom 24 kA switch[36] and a 4 farad capacitor bank which supplied voltage pulses of up to 200 V between a 50% transparent molybdenum anode and a Lanthanum Hexaboride cathode[10] (Fig. 10). The electron temperature measured with Langmuir probes and Thomson scattering varied between 1 and 8 eV depending on discharge conditions. For these experiments, $T_e \approx 4$ eV. The ion temperature was measured using a McPherson 1.3 m monochrometer examining the deconvolved widths of HeII lines at 320.3 nm. $T_i \approx 2$ eV. The wave-launch antennas were driven using a transistor-based RF circuit which delivered 200 A at 500 V_{pp} to the coils. The antennas were powered by high voltage switching transistors; therefore, the voltage waveforms were square waves switching from positive to negative polarities. To ensure the highest power to the antennas, a tuned circuit comprising the antenna inductance and an external match capacitor (typically 0.22 μF) was used. The current to each of the straps was monitored with calibrated current sensors. The current and the magnetic field measured with B-dot probes were sinusoidal. In some previous experiments $\left(\frac{\delta B_\perp}{B_{0z}} \approx 10^{-3}\right)$ in the far field of the antenna which was less than 1/100 of the field for nonlinearities to appear. The magnetic field of the resultant shear waves had an amplitude of less than 1 G. For the present experiment, Fig. 3 presents a typical waveform of one component of the measured magnetic field. The waves are in the linear regime. In this case $B_{0z} = 400$ G, $f = 95$ kHz, $= \lambda_\perp = 8$ cm, $\lambda_{||} = 112.5$ cm, $n_e = 1.25 \times 10^{13}$ cm^{-3} and $v_A = 1.6 \times 10^7$ cm/s.

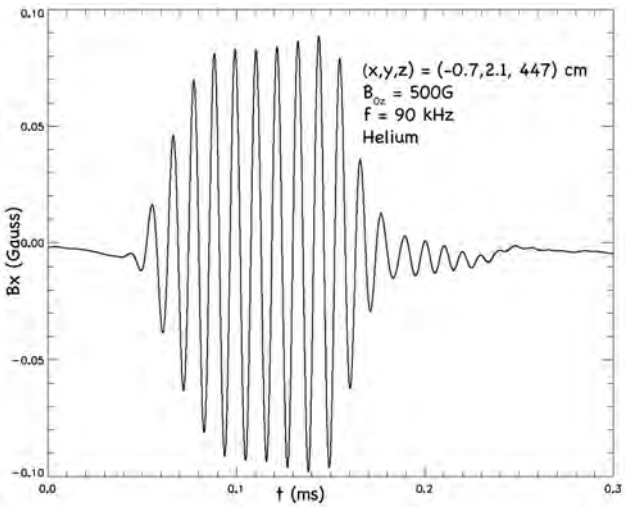

FIG. 3. One component, B_x, of the wave magnetic field during an RF tone burst. This is the time-integrated signal from a "Bdot" probe. The wave was switched on 30 ms into a 40 ms, 7.4 kA discharge. Time here is measured as $t = 0$ is the time the antenna is switched on. The maximum wave field measured was 0.25 G peak. Here, the center of the machine is at $(x, y) = (0, 0)$ and z the distance from the end of the device as shown in Fig. 10.

III. THEORY

A. Antenna modeling

We next discuss the physics of how shear Alfvén waves are launched from loop antennas. The magnetic field of shear waves is accompanied by a three-dimensional current system.[12] The parallel currents are carried by electrons, and the cross field current required to close the system (polarization current) is carried by the ions. This has been established with direct measurement in an earlier publication.[37] In the fluid picture, the wave is generated by plucking magnetic field lines transverse to the background field, much as one does with a guitar string. This is misleading. A far better way to describe wave generation starts with an oscillating field-aligned current filament at a frequency below f_{ci}. When the width of the current channel is of the dimension of the electron skin depth (c/ω_{pe}) or the ion sound

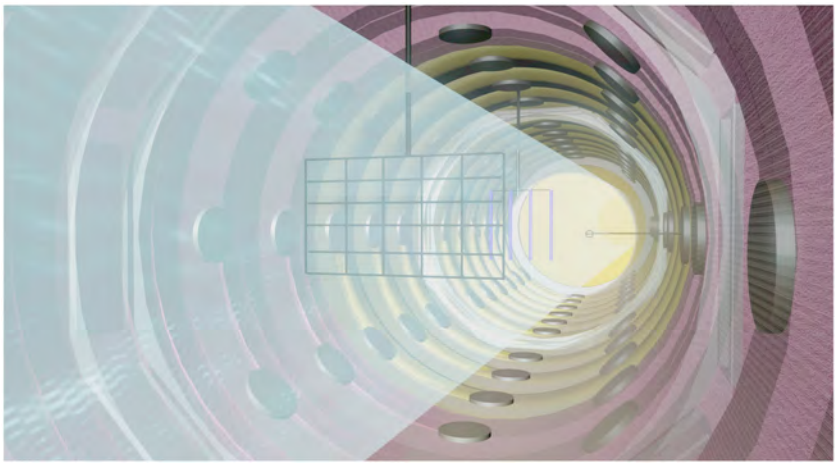

FIG. 2. A schematic CAD drawing (not to scale) of the tennis racket and a four-strut antenna in the LAPD device. The plasma column is represented in blue. A three-axis magnetic field probe is shown on the right, and the fork launcher is visible in the distance. The LaB_6 cathode at emission temperature is shown at the rear. The inner diameter of the chamber is 1 m. A number of ports are visible.

FIG. 4. (a) End on view of a single current loop. At one instant of time the current comes out of the page on top of the loop and into the page on the bottom. The background magnetic field direction is out of the page. (b) 3D CAD drawing of orthogonal loops indicating the generation of cones.

gyroradius (v_{Te}/ω_{ci}) Alfvén wave cones are formed. The expression for the magnetic field of the radiated wave for cold ions was derived by Morales and Maggs[38] and is given below. The formalism was extended to hot ions by Vincena *et al.*[39] That paper illustrates that wave effects due to hot ions are minor in the propagation band below the ion cyclotron resonance (as is the case for this experiment),

$$b(\rho,\xi) = \int_0^\infty dK \frac{J_1(K)}{k} J_1(K\rho) \exp\left\{ i\xi \left[\frac{1 + i\Gamma_\parallel (K/p)^2}{1 + (K/s)^2} \right]^{1/2} \right\}, \quad (1)$$

where the dimensionless variables are

$$b(\rho,\xi) = \frac{acB_\theta}{2I_0}, \quad (2)$$

$$\rho = \frac{r}{a}, \quad \xi = k_A z, \quad (3)$$

$$K = ka, \quad \Gamma_\parallel = \frac{\nu_e}{\omega}, \quad (4)$$

$$p = \frac{a\omega_{pe}}{c}, \quad s = \frac{a}{\rho_s}. \quad (5)$$

Here, k is the perpendicular wavenumber; J_1 is the Bessel function of the first kind of order 1; ν_e the electron collision frequency; a the radius of the current channel; ρ_s the ion sound gyroradius; $k_A = \omega/v_A$; I_0 the magnitude of the current in the wire; ω_{pe} the electron plasma frequency; and B_θ the magnetic field of the radiated azimuthal wave. Initial experiments that applied oscillating voltages to small grids generated Alfvén wave cones.[29,30,40] Since then, rotating magnetic field (RMF) antennas have been developed[12] and widely used in LAPD. A loop antenna generates shear waves in the following way. The RMF antenna is shown schematically in Fig. 4.

In this case, the area of the wire shown transverse to the background magnetic field in Fig. 4(a) takes the place of the mesh grid used to generate waves in the initial experiments. In this experiment, the wire diameter was 2 mm and the loop diameter ≈ 8 mm. The magnetic field of the waffle antenna is constructed by adding the complex magnetic field from 5181 loops. This is illustrated step by step. A calculation using theory by Morales and Maggs[38] for each 2 mm cone source using Eq. (1) is shown in Fig. 5. In both the experiment and theoretical

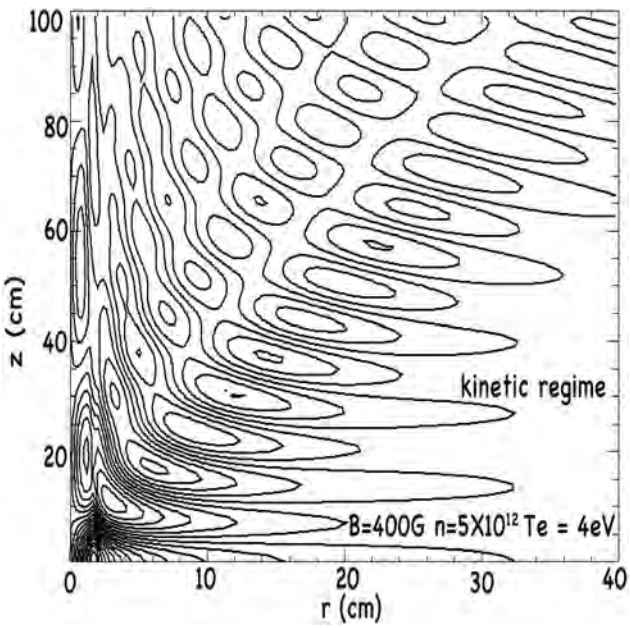

FIG. 5. Magnetic field lines calculated for a 2 mm diameter current source. The abscissa is the radial direction and ordinate is distance from the source in cm. The field is symmetric about rotation in ϕ, that is about the z direction.

analysis the magnetic field used was $B = 400$ G, density $n = 4.5 \times 10^{12}$ cm^{-3}, $T_e = 4.0$ eV and $\nu = 4.5 \times 10^4$ s. The pattern is symmetric about the z axis, and the 2D pattern is constructed with this in mind. The coordinate system was then changed from cylindrical to rectangular. A single loop comprises two side-by-side "cone" generators is illustrated in Figs. 4 and 6. The currents shown in Fig. 6 are separated by $\delta x = 8$ mm. The oscillating currents on the edge of Fig. 6(a) are π out of phase; therefore, the magnetic field between them is enhanced by constructive interference. A single vertical strut of the antenna comprises six sections, each having 24 loops. The calculated pattern showing the magnitude of the field generated from a single vertical strut is shown in Fig. 7. The magnetic field of the wave is aligned

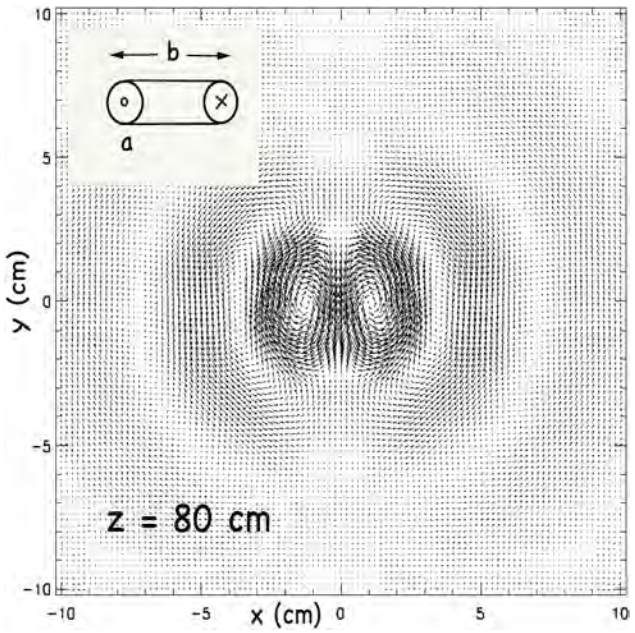

FIG. 6. Calculated vector magnetic field of two-cone current sources side by side in the x direction. (Inset) Schematic of the loop where the wire diameter is $a = 2$ mm and the loop diameter $b = 8$ mm.

with the background field, and the largest field is colored red. Finally, a figure showing the theoretical results of the antenna with six horizontal and six vertical struts is given in Fig. 8. In the experiment (and theory) alternate columns and rows are phased 180 degrees apart. The resultant pattern is one in which the magnetic field between struts is a result of destructive or constructive interference. This was first seen in Ref. 35 with antennas of two and ten vertical struts wound in much the same way. The corresponding wave numbers are $k_x = 0.84\,\mathrm{cm}^{-1}$, $k_y = 1.4\,\mathrm{cm}^{-1}$, and $k = 1.6\,\mathrm{cm}^{-1}$. In this case $k\rho_s = 1.6\,\mathrm{cm}^{-1}$ and $k\rho_i = 0.82\,\mathrm{cm}^{-1}$. The theoretical k spectrum for the waffle antenna in the x-y plane is displayed in Fig. 9.

IV. EXPERIMENTAL RESULTS

A. Magnetic field with a single waffle antenna

Three-axis, 10-turn magnetic field probes[41,42] (Bdot) were used through side ports 32 cm axially apart. Data were acquired at 55×55 (3025) transverse locations with $\delta x = \delta y = 0.7$ cm. In the first data run, a single, eight struts (eight rows and eight columns) antenna was placed at $z = 384$ cm and the Bdot probe at $z = 447$ cm. Each strut had 460 turns of wire, two levels deep. The typical antenna current was 70 A peak. The Bdot probes were differentially wound, and the difference signal was amplified by 10. A five-shot average was taken at each location. The background magnetic field, B_{0z}, was 500 G. Helium gas was puffed into the source on each shot, the discharge current and voltage were $I_D = 7365$ A, $V_D = 85$ V; V_D is the cathode–anode voltage. The placement of the antennas in machine coordinates is given in Fig. 10. The wave was launched 30 ms into a 40 ms discharge. Plasma density was measured with two axially spaced 300 GHz microwave interferometers and was $n_e = 6 \times 10^{12}\,\mathrm{cm}^{-3}$. The density profile is measured by Langmuir probes that are calibrated by the

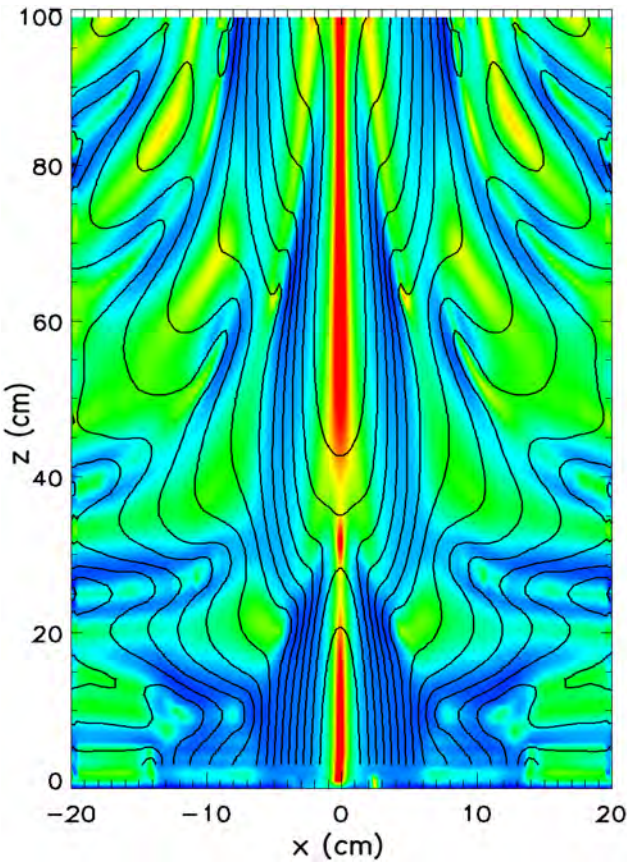

FIG. 7. Theoretical calculation of the magnitude of $log(B_{wave})$ as a function of x (transverse distance) and z (distance along the background magnetic field. The log was used in the display to bring out smaller features. The vertical struts are located at $x, z = 0$ and are transverse to the plane in this figure. Each strut consists of two layers, each with 144 wires stacked along y. Each wire has a diameter of $a = 0.2$ cm and is the source of an Alfvén cone. The vertical strut is located at $x = y = 0$. Here $B = 400$ G, $n = 5.0 \times 10^{12}\mathrm{cm}^{-3}$, $T_e = 4$ eV. Contours are drawn to guide the eye.

interferometers. The plasma was fired every 3 s to allow for gas evacuation between shots. Data were acquired at 8192 time steps, $\delta t = 80$ ns. A typical trace of the magnetic field at one location is shown in Fig. 3. The probes are sensitive to the time varying magnetic field; therefore, after any offset was removed, every component of the Bdot data at each location was integrated in time. The signals were subsequently digitally filtered to remove high frequency noise. Alfvén waves below the ion cyclotron frequency ($f_{ci} = 152$ kHz) were launched by all antennas at the same frequency ($f = 95\,\mathrm{kHz} \approx 0.63 f_{ci}$).

In all cases, a tone burst of 10–20 cycles was launched from each antenna. There were two RF sources, run 180 degrees out of phase, and feeding alternate struts. Each antenna was switched on with a pulse generator (Stanford SRS-DG535), which then activated two arbitrary waveform generators (Agilent 3322 A). Each arbitrary waveform generator (AWG) supplied waveforms to be amplified to two RF boxes, one for horizontal and the other for vertical struts. The AWGs also controlled the waveform phases. The current to each strut was measured with Pearson current monitors, and the current waveforms

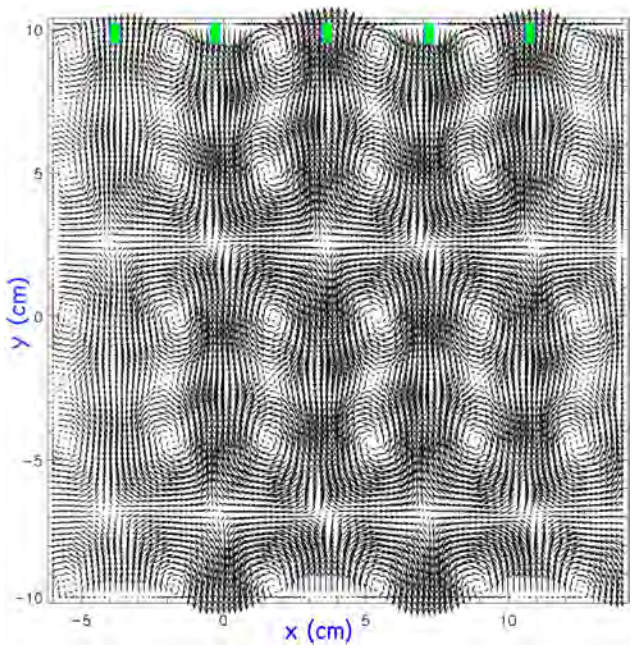

FIG. 8. Magnetic field, predicted by theory, due to the all the struts in the 6 × 6 waffle antenna at $z = 20$ cm shown. The positions of the five out of six struts are denoted by green bars. The horizontal and vertical struts extend from −12 to 12 cm. They are located in the center of the "O" points. Each horizontal and vertical strut is π out of phase with its neighbor. There is also an overall phase difference of π between the horizontal and vertical struts. This should be compared to Fig. 11, which is experimental data.

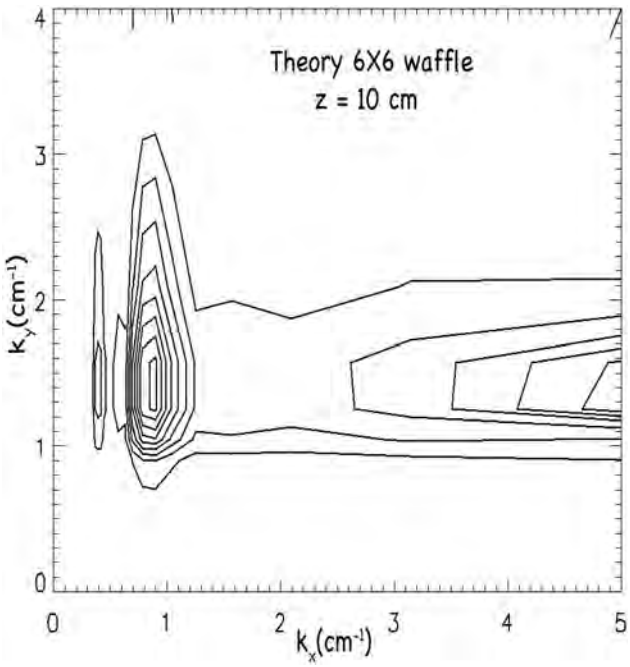

FIG. 9. Wave numbers calculated using a spatial Fourier transform of the magnetic field shown in Fig. 8. The corresponding dominant wavelengths are $\lambda_x = 7.85$ cm and $\lambda_y = 4.19$ cm. This was calculated for $z = 10$ cm from the waffle antenna.

were displayed on an eight-channel, 2 GHz scope (LeCroy-HD 8208). The voltages were monitored with high voltage probes (Tektronix P6015A). Data were digitized with a Struck Innovative Systems 32-channel 100 MHz digitizer.

Magnetic field vectors in the plane at $z = 415$ cm are shown in Fig. 11. Magnetic vortex-like structures are clearly visible indicting multiple parallel currents. The distance between "O" points is about 7 cm, the perpendicular wavelength is twice that, therefore $k_\perp \cong 0.9\,\mathrm{cm}^{-1}$. The relevant parameters are: $k_\perp \rho_i = 1.0$, $k_\perp \rho_s = 0.9$, and $k_\perp \lambda_i = 12.6$ where ρ_i is the ion gyroradius based on a 4 eV ion temperature ($\rho_i = 1.1$ cm and $\rho_s = 1$ cm under these conditions) and λ_i the ion inertial length. At higher densities, $k_\perp \lambda_i$ can be as low as 7. The magnetic field of the antenna yields $\frac{\delta B}{B} \cong 0.5\%$, far too small to expect nonlinear effects such as those caused by the ponderomotive force.

A second antenna with four horizontal and four vertical struts was also constructed. The background magnetic field was 500 G, the wave frequency was 112.5 kHz and the density $n \approx 1.1 \times 10^{13}\ \mathrm{cm}^{-3}$. The strut spacing was 4 cm, the antenna current was 131 A_{p-p} and the wave magnetic field 1.2 m from the antenna was of order 0.25 G. The current is shown as a contour plot, and magnetic field vectors are constructed as a function of time in a movie (online) of Fig. 12

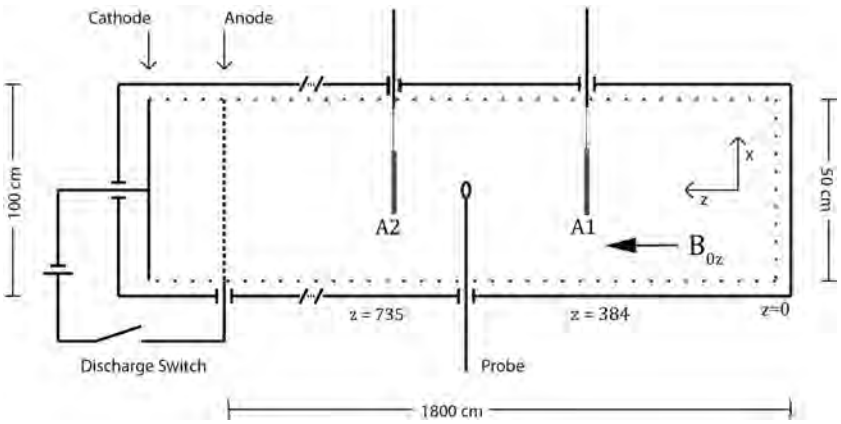

FIG. 10. Schematic of machine and placement of two antennas and diagnostic probe (not to scale). A1 and A2 are antennas which are both waffles or a fork and waffle depending on the experiment. Not to scale.

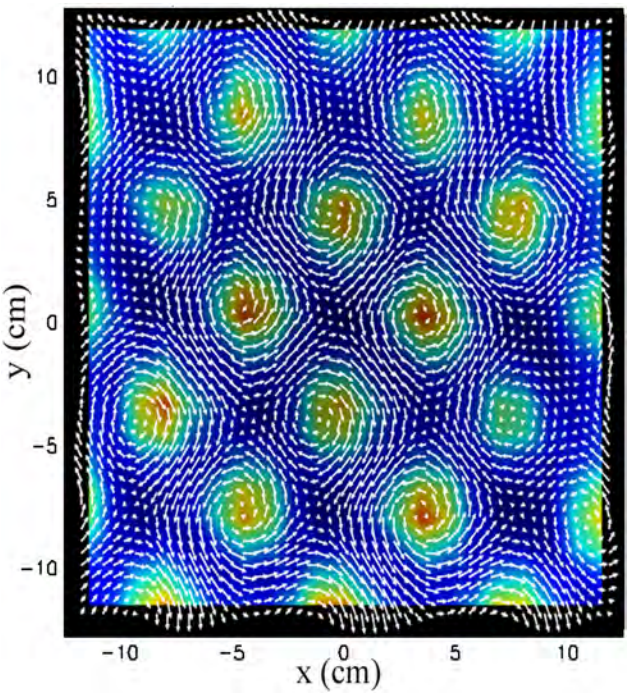

FIG. 11. $B_x - B_y$ vectors at $z = 415$ or 32 cm from the waffle antenna. The largest magnetic field in this plane is 0.162 G. The largest field recorded in these data set is 0.25 G. The length of each arrow is proportional to the value of the wave field at that point. Also shown is the current depicted as a shaded surface. The distance between the "O" points of the wave is approximately 4 cm or one half the transverse wavelength.

(Multimedia view). Each time step in the movie is 80 ns; the wave was on for 150 μs.

B. Magnetic field with the waffle and fork antennas

Experiments with a vertical four-strut "fork" antenna and 8 × 8 strut "waffle" antenna were conducted, and subsequently with two waffle antennas with different strut spacings. In the fork and waffle study, the background density was $n = 1.5 \times 10^{13}\,cm^{-3}$, $B_{0z} = 400$ G ($\frac{f}{f_{ci}} = 0.64$) with $f_{wave} = 95$ kHz. The four-strut fork antenna was inserted at z = 734.9 cm and a 6 × 6 strut waffle antenna at z = 383.4; their separation was $\delta_z = 351.5cm$. In Fig. 3 *A*1 is the waffle and *A*2 the fork. The waffle struts were spaced 4 cm apart, yielding $k_{xw} = k_{yw}\,0.785\,cm^{-1}$. Here k_{xw} is the wave number in x for the waffle antenna. The Rf current applied to the waffle struts was $75\,A_{peak}$, and alternate struts were out of phase by π. The fork antenna had four struts spaced 2.54 cm apart with $k_{xf} = 1.24\,cm^{-1}$. The vertical wave number based on the 22 cm length of the fork tines is $k_{yf} = 0.143\,cm^{-1}$. High frequency noise in the Bdot probes caused by the transistor switches was eliminated with a combination of a 300 kHz filter and an SRS (Stanford Research Systems) active filter set for $f < 209$ kHz. The magnetic fields from the waffle antenna in this experiment were lower than in the first experiment. In this case, the largest field was 50 mG peak in spite of antenna currents of the order of 75 Amp-peak. The current in the fork antenna was 90 A peak, and close to it the wave magnetic field was larger, topping out at 0.25 G.

Five transverse planes of the magnetic field were acquired between the antennas. The magnetic field close to the waffle and fork antennas is shown in Fig. 13. The time at which the figures are displayed was chosen to make the pattern clearest. Close to either antenna, the pattern can be clearly identified with the structure of the antenna. The pattern becomes interesting between the antennas where the waves are superposed.

The Alfvén wave currents can easily be calculated using the differential form of Ampère's law. They are shown in full three dimensions at one time in Fig. 14 (Multimedia view). This figure also contains a movie showing the time evolution of the axial current density as a function of space. The magnetic field close to either the waffle antenna or the fork reflects their geometry as seen in Fig. 13. Midway between the antenna, the pattern is ever changing and reflects what may be a superposition of them, although new modes are present, as will be shown in a subsequent section. The vector magnetic field pattern at one instant of time is shown in Fig. 15 (Multimedia view). This is best appreciated in a movie of this figure, which may be obtained online from the link in the figure. The maximum parallel current density at z = 703 cm (32 cm from the waffle antenna) at time $\tau = 1.332$ ms into the wave is 68 and 113 mA/cm^2 at z = 415 cm.

C. Experimental wave numbers

The magnetic field for the four-strut fork and 8 × 8 strut waffle antennas was measured on five planes transverse to the axial magnetic field. The data were then linearly interpolated to nine planes. The wavenumber data were obtained both as a function of time and temporally averaged. In the first case, the data were Fourier analyzed in space on each plane and for each component. The now complex data had the form B[t, k_x, k_y, z, ic] where z represents one of the planes transverse to the background magnetic field and ic is the x, y, or z component of **B**. The time averaged magnetic field was then calculated. To do this, an FFT was calculated for each component at every position. The Fourier components centered on the wave frequency were summed. The inverse Fourier transform was then employed to calculate the complex time averaged quantity $B[k_x, k_y, z, ic]$, the temporal average. This, in turn, was used to calculate the time averaged wavenumber spectra on each plane and for each component. Figure 16 shows the wave numbers averaged over the spectra of the Fourier components: B_x, B_y, and B_z. The dominant wave numbers close to the waffle antenna are $k_x = 1.5\,cm^{-1}$ and $k_y = 0.25\,cm^{-1}$ as well as $k_x = 1.5\,cm^{-1}$ and $k_y = 5.5\,cm^{-1}$. The dominant component k_x is 1.9 times larger than the theoretical prediction, but a second component at $(k_x, k_y) = (0.5, 1.0\,cm^{-1})$ is close to the theoretical values shown in Fig. 9. The wave numbers close to each antenna are what might be expected from Fig. 13. A factor complicating the comparison of experiment and theory is that the plasma density close to the antenna is not uniform. The density profile has 10 percent dips, which line up with the antenna struts, and the Alfvén wave speed and propagation are density dependent. In the theoretical calculation, the density is constant in space. Close to the antennas, the identification of wave numbers is straightforward. Using a two-dimensional Fourier transform of the data for the fork antenna, the dominant wave numbers are $k = k_x = 0.51\,cm^{-1}$ with $\lambda_x \approx 6.2$ cm and k_y undefined. The theoretical wave numbers associated with the waffle antenna (Fig. 1) are the same for B_x and B_y, $k_x, k_y = 0.785\,cm^{-1}$ corresponding to a wavelength of 6 cm. The dominant wave number for B_y is the same

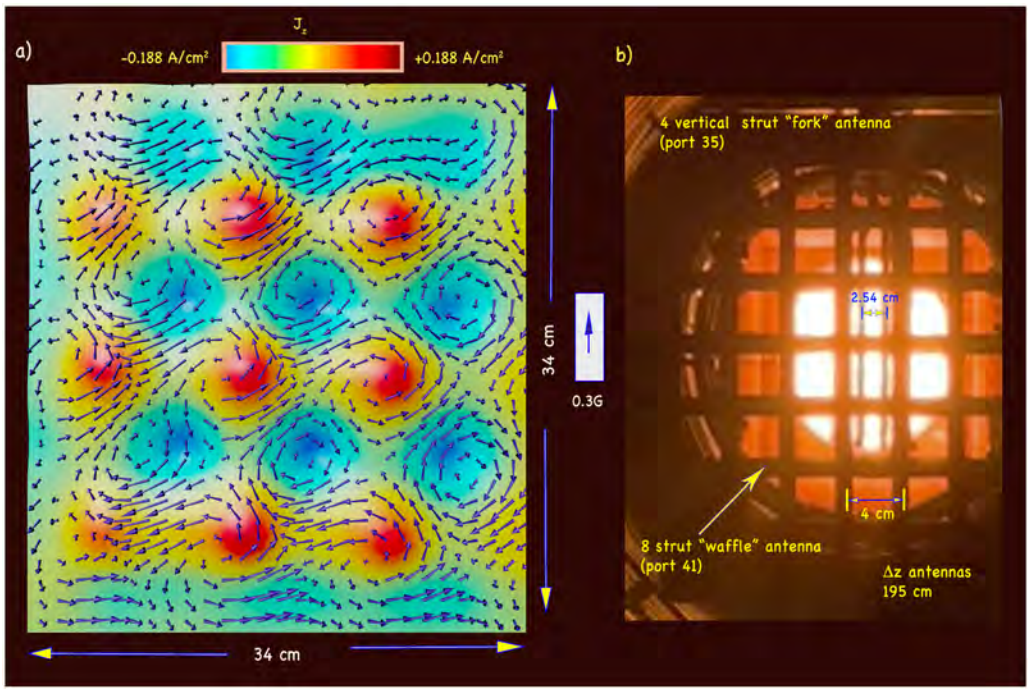

FIG. 12. (a) Surface map of shear Alfvén wave current. The time evolution of the current ($\delta t = 80$ ns) is shown in a movie, which may be downloaded. Here, the background magnetic field is 500 G, f = 112.5 kHz, n = 1.1×10^{13} cm^{-3}, $\delta z_{antenna-probe} = 128$ cm. (b) Photograph of the waffle antenna in the machine seen from a window at the end of the LAPD (also see Fig. 11). Multimedia available online.

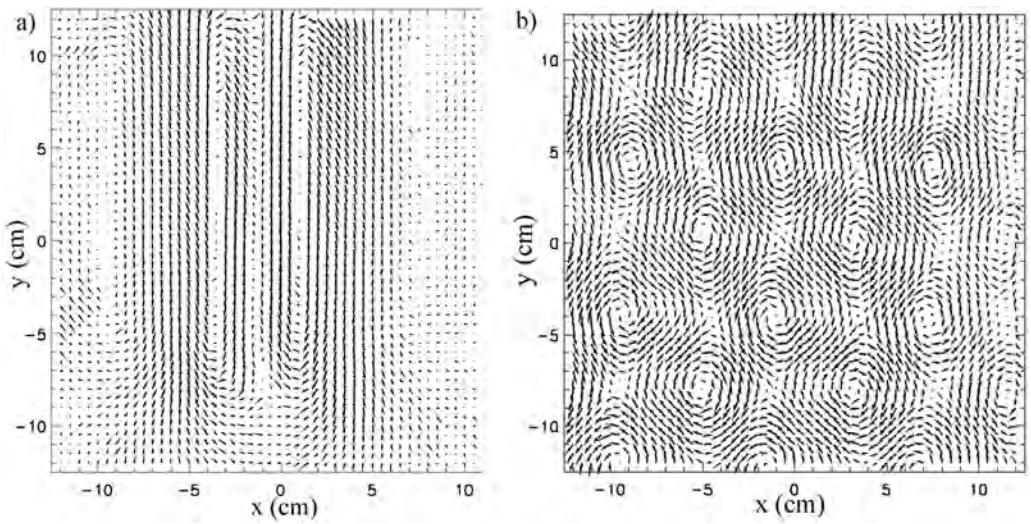

FIG. 13. Magnetic field vectors B_x, B_y on two planes. The antennas were a 4 vertical strut fork and an 8 × 8 strut waffle. (a) Vector field at $z = 415.4$ or 32 cm from the fork antenna at $t = 1.275$ ms. (b) Vector field at $z = 703$ or 32 cm from the waffle antenna at $t = 1.264$ ms.

as that for B_x. A second wave number corresponding to a smaller magnetic field is present at $(k_x, k_y = 0.26\,\text{cm}^{-1})$ with a corresponding wavelength of 15.4 cm. Midway between the antennas the magnetic field is complicated, and many additional wave numbers, all of which correspond to shear waves, are present. When the wave numbers are averaged over the entire RF burst, many modes exist in three dimensions and are displayed in Fig. 17. However, the wave number spectra evolve with time. At early times, just after wave turn on, there are a few modes and they are small. The k-spectrum at t = 162 μs after the beginning of the wave is shown in Fig. 17. The

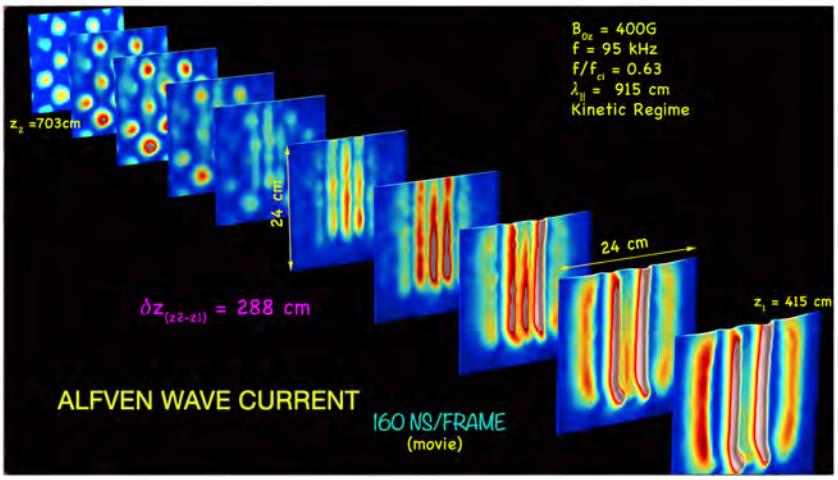

FIG. 14. Data at one instant of time showing 3D currents of the Alfvén waves. Data were acquired at 3025 locations on each of five planes. The data shown was interpolated to 9 planes. A movie with temporal resolution of 160 ns/frame is available in the online version of this manuscript. Data were acquired at 80 ns intervals. The pattern close to either antenna is what one would expect. In the center both waves are heavily damped, and the pattern is a complicated function of space and time. Multimedia available online.

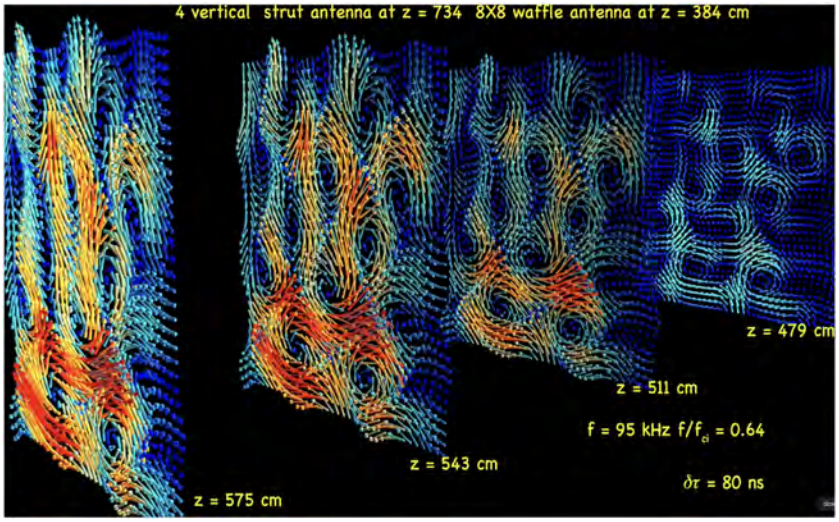

FIG. 15. Magnetic field at several axial locations at time $\tau = 1.12$ ms. The length of the arrows depicting the magnetic field is proportional to its magnitude. Note the data plane closest to the waffle antenna is at $z = 479$ cm. The antenna is at $z = 384$ cm. The "fork" antenna is at $z = 734$ cm, and therefore, this is a small part of the region between them. The mode structure changes in time leading to a complicated time-dependent wave number spectrum. Multimedia available online.

mode structure constantly changes in time, where $t = 0$ corresponds to the beginning of the Alfvén tone bursts (fork and waffle) that are on for 30 periods or 230 μs. At $t = 0$ there are a few modes and they are small. In Fig. 17 the k_x and k_y axes correspond to perpendicular wavenumbers. The δz axis indicates the position between the antennas. The diameters of the red spheres in Fig. 17 are proportional to the strength of the modes. The white spheres are the modes when the wave field is averaged over the burst. They are drawn on the same scale.

D. Two waffle antennas

Magnetic field data were acquired using a three-axis B-dot probe with two waffle antennas in the plasma. The first antenna had eight struts in the vertical and horizontal directions, and the second was a 6×6 matrix. The antennas were 352 cm apart in the axial direction (z). In this case, the background magnetic field was $B_{0z} = 400$ G, and the average density measured by two interferometers spaced 2 m apart was 1.25×10^{13} cm^{-3}. Data were acquired at 80 ns intervals. As in the previous run, a 2.5 MHz low pass filter was used in conjunction with differential amplifiers with a gain of 100. The wave frequency was $f_{wave} = 97.5$ kHz and the wave was on for 408 μs. The current in each of the eight struts in the first antenna was $120A_{peak}$ at $400V_{pp}$. The current in the six-strut antenna was 144_{peak}. The rf applied to adjacent struts was 180 degrees out of phase on each antenna. In addition, the two antennas were driven 180 degrees out of phase with respect to each other. The six-strut antenna was at $z = 734$ cm and the eight-strut antenna at $z = 384$ cm. A limited dataset acquired on one transverse plane at $z = 479$ cm as the six-strut antennas developed an internal arc soon afterwards. The magnetic field when both antennas are on is shown in Fig. 18 (Multimedia view). A movie showing the field as a function of time is available online. The three-dimensional field, wave currents, and mode structure are expected to be more complicated than the fork and waffle. The axial plasma current in the plane was

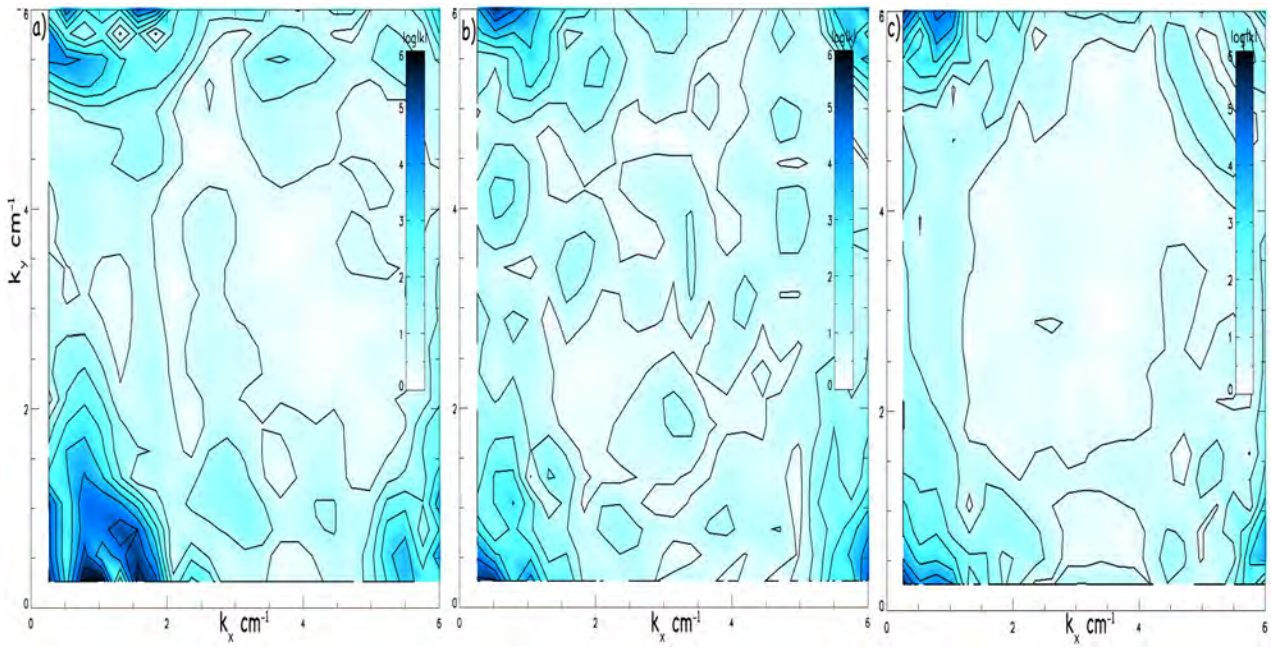

FIG. 16. The log of wave number spectra (in arbitrary units) due to the presence of both antennas and averaged over time is displayed on three transverse planes. Plotting the log of the spectra brings out the smaller modes. A color map is shown on the right, and the darkest color corresponds to the largest modes. (a) Spectra at z = 416 cm ($\delta z = 0$). (b) Spectra at z = 576 cm ($\delta z = 160$ cm). (c) Spectra at z = 672 cm ($\delta z = 256$ cm). The plane at z = 416 cm is 32 cm from the waffle antenna which is at z = 388 cm, and the plane at z = 672 cm is 32 cm from the fork antenna.

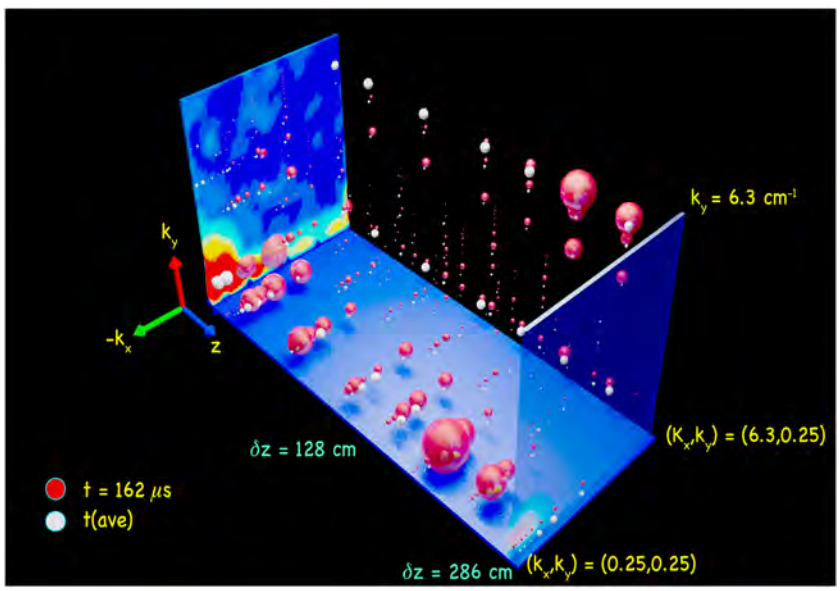

FIG. 17. The measured three-dimensional wave number spectra due to the presence of both antennas. Two sets of modes are displayed. The first shown as red spheres was acquired at a given time, $t = 168\mu$s into the burst. The white spheres denote the spectra averaged over the time the wave burst is on. Each sphere denotes a mode. The two sets of spheres are on the same scale. The radius of each sphere is proportional to the strength of the mode. Two of the axes are the transverse wave numbers (k_x, k_y) and the third is the relative location in z, i.e., the position along the background magnetic field. Here, z is given as positions relative to the first plane, $z = 0$ ($z = 416$ cm in machine coordinates) which is closest to the "waffle" antenna located at $z = -32$ cm. The furthest plane $z = 286$ cm ($z = 700.6$ cm in machine coordinates) is closer to the "fork" antenna. The three cut planes, two at the extreme z positions and one at $k = 0$ are surfaces of the time averaged mode-numbers. The bright colors denotes the magnitude of the modes.

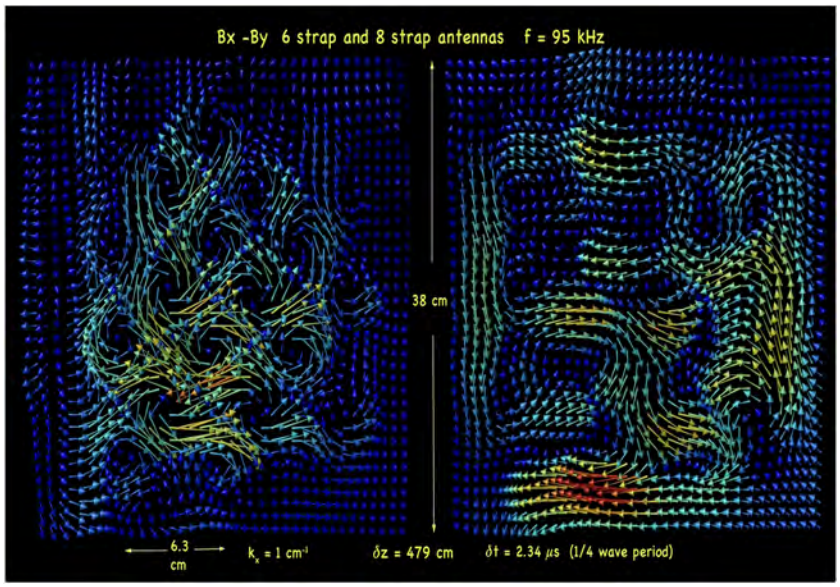

FIG. 18. The magnetic probe is located at z = 479 cm: $\delta z_{6strut} = 255$ cm and $\delta z_{8strut} = 95$ cm the distances to the probe plane. The "6 × 6 strut waffle" antenna is at z = 734 cm, the "8 × 8 strut waffle" antenna is at z = 384 cm. The two figures are shown 1/4 of the wave period apart. The magnetic field rapidly changes in time and space and can be appreciated in a movie, which may be downloaded. Multimedia available online.

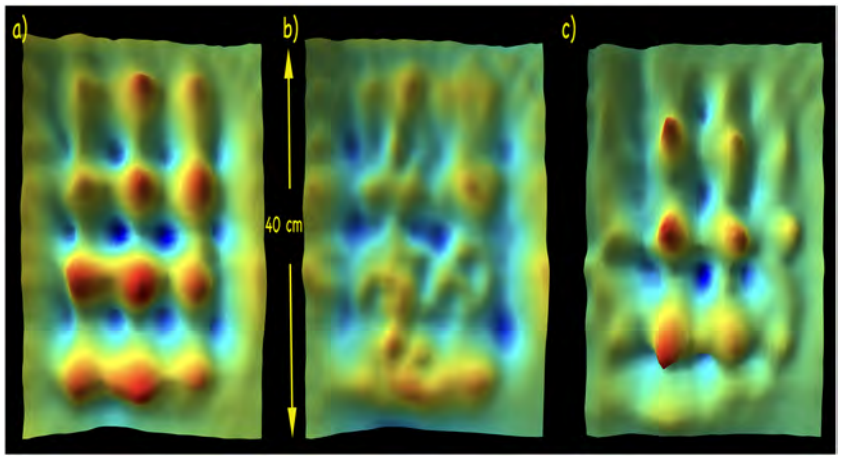

FIG. 19. The Alfvén wave current at three times during the wave period. Data were acquired at a cadence of 0.8 μs. (a) Current at $\tau_1 = 5.243$ μs after antennas are switched on (b) current at $\tau_1 + 1.282$ μs, (c) current at $\tau_1 + 2.883$ μs. The wave period is $\tau_{wave} = 10.026$ μs. The wave current, j_z is on the order of 50 mA/cm^{-2} in the wave maxima.

calculated using Ampère's law $\nabla \times \vec{B} = \frac{4\pi}{c} j$. In CGS the voltage and current are expressed in statvolts and statamps, but here we convert them to the more common volts and amps. The Alfvén wave current at three times during the wave period is shown in Fig. 19. As time goes on, the wave field on this plane goes to zero [Fig. 19(b)] and the pattern alternates between six and eight maxima/minima. This can be seen in the movie. The two-waffle case is of great interest and will be pursued in future experiments.

E. Summary and conclusions

There is great interest in generating large amplitude shear Alfvén waves. The theory[16,17,19,20] estimates that density changes due to ponderomotive force and induced plasma flows occur when $\frac{\delta B_{wave}}{B} \approx 10\%$ (here an unattainable 40 G). Steepening of large amplitude waves in a dense pulsed plasma has been observed.[43] We propose that shear waves of modest amplitudes $(\frac{\delta B}{B}) \approx 1\%$–$2\%$ can lead to chaotic ion orbits in the wave fields. The $k_\perp \rho_s \approx 1$ waves generated here may be able to do that. The requirement is that $E_\perp$ of the wave be sufficient to give an ion a kick out of the wave current channel within one cycle, moving it into a magnetic null.

The presence of the modes shown in Fig. 17 is not the result of nonlinear processes. They are simply interference patterns from "cone" magnetic fields emanating from thousands of sources. The shear wave dispersion in the kinetic regime is given by[38]

$$\frac{\omega^2}{k_\parallel^2} = v_A^2 \left(1 - \bar{\omega}^2 + k_\perp^2 \rho_s^2\right). \tag{6}$$

The perpendicular field for kinetic shear waves is[44]

$$E_\perp = \frac{v_A}{c} \frac{1 - \bar{\omega}^2}{\left(1 - \bar{\omega}^2 + k_\perp^2 \rho_s^2\right)^{1/2}} B_{\text{wave}}. \tag{7}$$

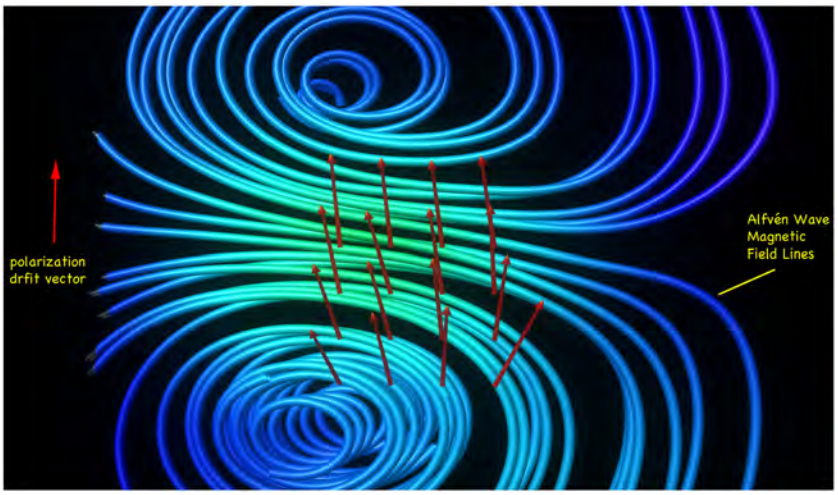

FIG. 20. LIF data capturing the ion motion at the moment when ions are crossing the background field to close the Alfvén wave current (taken from a survey paper on Alfvén waves by Gekelman *et al.*[37]). The background magnetic field (1.5 kG) and the direction of wave travel both point into the page. The magnitude of the drift varied between 1.33 and 8.34×10^4 cm/s. By comparison, the ion thermal speed for 0.77 eV ions in argon is 1.36×10^5 cm/s.

For this two-waffle experiment, the background field was 400 G, a representative perpendicular Alfvén wavelength of 5 cm, $B_{\text{wave}} = 0.25$ G, $\bar{\omega} = 0.64$ and $\rho_s = 1.03$ cm, and the experimental parameter $\lambda_\parallel = 2$ m. Equation (7) gives the perpendicular electric field $E_\perp = 112$ mV/cm. This is similar to $E_\perp$ measured using laser induced fluorescence (LIF) in an experiment with an Ar plasma at a higher magnetic field, $B_{0z} = 1.5$ kG. The motion of ions was tracked in the LIF experiment. In that study, the shear wave amplitude was of the order of 0.6 G, $\frac{\delta B}{B_{0z}} \approx 10^{-3}$ where $B_{0z} = 1.5$ kG and the plasma density was lower $n \approx 5.0 \times 10^{12}$ cm^{-3}. LIF has never been achieved with He ions.

The parallel electric field can be estimated from this perpendicular field using the relationship[44]

$$E_\parallel = \frac{ik_\perp k_\parallel \rho_s^2}{(1-\bar{\omega}^2)} E_\perp. \tag{8}$$

For $k_\perp = 0.63$ cm^{-1} measured in the previous Argon experiment.[44] In the Ar experiments $E_\parallel = 2.9$ mV/cm. In this experiment, it is 4 mV/cm. The parallel current of a shear wave is carried by the electrons, but the ion polarization drift v_p closes the current,

$$v_p = \frac{c}{\omega_{ci} B_{0z}(1-\bar{\omega}^2)} \frac{dE_\perp}{dt}. \tag{9}$$

In general, the $\vec{E} \times \vec{B}$ motion of the electrons and ions together leads to no net current, except in a narrow range where the wave frequency is near the ion cyclotron frequency (as described by Morales *et al.*[28])

$$v_{\vec{E}\times\vec{B}_{0z}} = \frac{c}{B_{0z}^2} \frac{\vec{E}_\perp \times \vec{B}_{0z}}{(1-\bar{\omega}^2)}. \tag{10}$$

The LIF experiments are instructive: a specialized optical probe was used to allow motion to be detected in volumes of several cubic millimeters. The measured ion temperature was $T_i = 0.8$ eV. The shift of the Maxwellian distribution was used to calculate the ion drift velocity. Measurement details are given in Ref. 44. LIF and magnetic field measurements were made on four planes transverse to B_{0z}. The magnetic field has two "O" points indicating current channels similar to those in Fig. 6 and detailed in the RMF antenna paper by Gigliotti *et al.*[12] As the wave passes the probe the ions move in accordance with the ion polarization drift Eq. (9), the $\vec{E} \times \vec{B}$, or a combination depending on the phase. The wave period was 28 μs, and the polarization current occurs every half wave period. The ion polarization drift is shown in Fig. 20 and agreed well with the theoretical value in Eq. (9). The measured $\vec{E} \times \vec{B}$ motion was used to calculate the perpendicular electric field using Eq. (10). $\vec{E}_\perp$ was 75.9 mV/cm at a distance of 66 cm from the antenna and dropped to 19.6 mV/cm at 475 cm from the antenna located at z = 0. The parallel wavelength was 890 cm. This is within a factor of two from the calculated $E_\perp$ in the two waffle antenna experiment.

In the current experiment with two waffle antennas, the parallel wavelength was $\lambda_\parallel = 1.57$ m. The measured wave magnetic field was low $B \approx 0.3$–0.7 G. There are numerous current channels, as in Fig. 19, with parallel currents in the range of 27 mA/cm^2 each flowing through an area transverse to the background field of ≈ 9 cm^2 for a total current of 237 mA in each filament. This must be matched by the ion polarization current.

Even without wave magnetic fields large enough to cause nonlinear effects, the possibility of chaotic ion motion is attainable. The chaos is driven by the wave electric field and the precise initial condition of the ion affected. When the perpendicular wavelength is on the order of the ion gyroradius, which would be the case for argon test ions, both the polarization and $\vec{E} \times \vec{B}$ drifts will move ions chaotically throughout the volume. A small ion beam using argon as a tracer has been constructed and will be employed as a future diagnostic. Future studies will determine the nature of the chaos. For example, stochastic heating of Argon ions by large amplitude drift Alfvén waves, observed using LIF,[45] was seen in a tokamak. Stochastic motion of electrons in a tokamak and the destruction of magnetic islands are long thought to be the cause of disruptions.[46] Electron motion could become chaotic in this experiment as well, provided the shear waves are large enough over a considerable length of the device. This happens in a regime in which the ion displacement due to the polarization drift becomes comparable to the wavelength of the drift-Alfvén mode. This could be the case in the waffle experiments at larger wave amplitudes. In the two waffle case, as well as the waffle and fork experiment, the distance from a current channel to the vicinity of a null is of order 2 cm. The largest wave

field is of the order $0.7G_{peak}$ and using Eq. (10) the E/B drift velocity is 2.1×10^4 cm/s, the ions drift 8 mm in a quarter wave period. We are off by about a factor of three. There are several ways to increase the length of the perpendicular ion drift. These include building an antenna that produces larger $k_\perp$ modes; driving the antenna at higher current to generate larger parallel electric fields to drive the cones; and increasing $\bar{\omega}$, which, in turn, will increase the $\vec{E} \times \vec{B}$ drift [Eq. (10)]. One can also explore launching larger amplitude waves in a denser hydrogen plasma at a lower background field. This will be the course of future experiments, possibly with the aid of PIC simulations.

What is the reason that the shear wave cannot reach arbitrarily large amplitudes? In general, the parallel electron current can be very high, but the dispersion [Eq. (8)] and the experiment show that the parallel electric field is about 1% of the perpendicular field. The polarization current depends on $E_\perp$. In Eq. (8), the denominator is of order 1 and $E_\perp$ is proportional to $E_\parallel(\lambda_\perp\lambda_\parallel/\rho_s^2)$. The quantities in parentheses cannot be changed by orders of magnitude. The ion sound gyroradius, ρ_s, cannot be arbitrarily small because that would remove the wave from the kinetic regime. The wavelength product is limited by the dispersion relation. Thus far, our conclusions are that the relatively small magnetic fields of the wave are, therefore, an issue of antenna coupling to the parallel electric fields of the Alfvén wave cones.

ACKNOWLEDGMENTS

The authors thank George Morales for his many comments and insights. The authors also thank Zoltan Lucky, Marvin Drandell, and Tai Ly for their expert technical support. This work was performed at the Basic Plasma Science Facility, which is a DOE Office of Science, FES collaborative research facility, and is funded by DOE (No. DE-FC02-07ER54918).

AUTHOR DECLARATIONS

Conflict of Interest

The authors have no conflicts to disclose.

Author Contributions

W. Gekelman: Conceptualization (lead); Data curation (equal); Formal analysis (lead); Visualization (equal); Writing – original draft (lead); Writing – review & editing (equal). **S. Vincena:** Visualization (equal); Writing – original draft (equal); Writing – review & editing (equal). **P. Pribyl:** Data curation (equal); Writing – original draft (supporting); Writing – review & editing (supporting).

DATA AVAILABILITY

The data that support the findings of this study are available from the corresponding author upon reasonable request.

REFERENCES

[1]R. Bingham, P. K. Shukla, B. Eliasson, and L. Stenflo, J. Plasma Phys. **76**, 135–158 (2010).
[2]S. Moriyasu, T. Kudoh, T. Yokoyama, and K. Shibata, Astrophys. J. **601**, L107 (2004).
[3]A. Verdini and M. Velli, Astrophys. J. **662**, 669 (2007).
[4]C. S. Salem, G. G. Howes, D. Sundkvist, S. D. Bale, C. C. Chaston, C. H. K. Chen, and F. S. Mozer, Astrophys. J. **745**, L9 (2012).
[5]O. Alexandrova, V. Carbone, P. Veltri, and L. Sorriso-Valvo, Astrophys. J. **674**, 1153 (2008).
[6]S. Whitelam, J. Ashbourn, R. Bingham, P. Shukla, and D. Spicer, Sol. Phys. **211**, 199 (2002).
[7]P. K. Shukla, L. Stenflo, and R. Bingham, Phys. Plasmas **6**, 1677 (1999).
[8]C. Chaston, C. Salem, J. Bonnell, C. Carlson, R. Ergun, J. Strangeway, and R. J. McFadden, Phys. Rev. Lett. **100**, 175003 (2008).
[9]K. Stasiewicz, P. Bellan, C. Chaston, C. Kletzing, R. Lysak, J. Maggs, O. Pokhotelov, C. Seyler, P. Shukla, L. Stenflo, A. Streltsov, and J. Wahlund, Space Sci. Rev. **92**, 423 (2000).
[10]W. Gekelman, P. Pribyl, Z. Lucky, M. Drandell, D. Leneman, J. Maggs, S. Vincena, B. Va Compernolle, S. K. P. Tripathi, G. Morales, T. A. Carter, Y. Wang, and T. DeHaas, Rev. Sci. Instrum. **87**, 025105 (2016).
[11]S. Vincena, T. A. Carter, D. W. Auerbach, and W. Gekelman, Bull. Am. Phys. Soc. **53**(14), UP6.005 (2008).
[12]A. Gigliotti, W. Gekelman, P. Pribyl, S. Vincena, A. Karavaev, X. Shao, A. S. Sharma, and D. Papadopoulos, Phys. Plasmas **16**, 092106 (2009).
[13]Y. Wug, W. Gekelman, P. Pribyl, and T. Carter, Bull. Am. Phys. Soc. **2004**, NP12-00012 (2024).
[14]W. Gekelman, S. Vincena, B. Palmer, N. P. Pribyl, C. Mitchell, and J. Maggs, Plasma Phys. Controlled Fusion **42**, B15 (2000).
[15]M. Zhou, Z. Liu, and N. F. Loureiro, Proc. Natl. Acad. Sci. U. S. A. **120**, e2220927120 (2023).
[16]T. Drozdenko and G. Morales, Phys. Plasmas **8**, 3265 (2001).
[17]T. Drozdenko and G. Morales, Phys. Plasmas **7**, 3177 (2001).
[18]T. Drozdenko, "Propagation of shear Alfvén waves in perturbed plasmas," Ph.D. thesis (University of California, Los Angeles, 2001).
[19]P. Shukla, L. Stenflo, R. Bingham, and B. Eliasson, Plasma Phys. Controlled Fusion **46**, B349 (2004).
[20]P. Shukla and L. Stenflo, Phys. Scr. **T60**, 32 (1995).
[21]P. Shukla, L. Stenflo, R. Bingham, and R. Dendy, J. Geophys. Res. **101**, 27449, https://doi.org/10.1029/96JA02646 (1996).
[22]P. Bellan and K. Stasiewicz, Phys. Rev. Lett. **80**, 3523 (1998).
[23]R. Lysak and Y. Song, J. Geophys. Res. **108**, 1327, https://doi.org/10.1029/2003JA009859 (2003).
[24]J. Schroeder, F. Skiff, G. G. Kletzing, C. A. Howes, T. Carter, and S. Dorfman, Geophys. Res. Lett. **2016**, 4701, https://doi.org/10.1002/2016GL068865.
[25]G. G. Howes, K. D. Nielson, D. J. Drake, J. W. R. Schroeder, F. Skiff, C. A. Kletzing, and T. A. Carter, Phys. Plasmas **20**, 072304 (2013).
[26]A. A. Schekochihin, S. C. Cowley, W. Dorland, G. W. Hammett, G. G. Howes, E. Quataert, and T. Tatsuno, Astrophys. J. Suppl. Ser. **182**, 310 (2009).
[27]S. Boldyrev and J. C. Perez, Astrophys. J. Lett. **758**, L44 (2012).
[28]G. J. Morales, R. S. Loritsch, and J. E. Maggs, Phys. Plasmas **1**, 3765 (1994).
[29]D. Leneman, W. Gekelman, and J. Maggs, Phys. Rev. Lett. **82**, 2673 (1999).
[30]W. Gekelman, D. Leneman, J. Maggs, and S. Vincena, Phys. Plasmas **1**, 3775 (1994).
[31]R. Lysak and Y. Song, J. Geophys. Res. **35**, L20101, https://doi.org/10.1029/2008GL035728 (2008).
[32]R. Lysak and Y. Song, Adv. Space Res. **28**, 813 (2001).
[33]N. Singh, J. Geophys. Res. **104**, 6999, https://doi.org/10.1029/1999JA900003 (1999).
[34]K. Stasiewicz, G. Gustafsson, G. Marklund, P. Lindqvist, J. Clemmons, and L. Zanetti, J. Geophys. Res. **102**, 2565, https://doi.org/10.1029/96JA03462 (1997).
[35]W. Gekelman, P. Pribyl, S. Vincena, S. W. Tang, and K. Papadopoulos, Rev. Sci. Instrum. **90**, 083505 (2019).
[36]P. Pribyl and W. Gekelman, Rev. Sci. Instrum. **75**, 669 (2004).
[37]W. Gekelman, S. Vincena, B. Van Compernolle, G. J. Morales, J. E. Maggs, P. Pribyl, and T. A. Carter, Phys. Plasmas **18**, 055501 (2011).
[38]G. J. Morales and J. E. Maggs, Phys. Plasmas **4**, 4118 (1997).
[39]S. T. Vincena, G. J. Morales, and J. E. Maggs, Phys. Plasmas **17**, 052106 (2010).
[40]S. Vincena, W. Gekelman, and J. Maggs, Phys. Rev. Lett. **93**, 105003 (2004).
[41]R. Loveberg, *Magnetic Probes* (Academic Press, 1965), Chap. 3, p. 69.
[42]E. Everson, P. Pribyl, C. Constantin, A. Zylstra, D. Schaeffer, N. Kugland, and C. Niemann, Rev. Sci. Instrum. **80**, 113505 (2009).
[43]F. Boley and P. R. Forman, Phys. Rev. Lett. **12**, 385 (1964).
[44]N. Palmer, W. Gekelman, and S. Vincena, Phys. Plasmas **12**, 072102 (2005).
[45]J. McChesney, P. Bellan, and R. Stern, Phys. Fluids B **12**, 3363 (1991).
[46]A. Rechester and M. Roesenbluth, Phys. Rev. Lett. **40**, 38 (1978).